Journal of Organometallic Chemistry 792 (2015) 6–12

Contents lists available at ScienceDirect

Journal of Organometallic Chemistry

journal homepage: www.elsevier.com/locate/jorganchem

Anomalous orbital admixture in ammine complexes☆

Tao Zeng, Kyle M. Lancaster, Nandini Ananth, Roald Hoffmann*

Department of Chemistry and Chemical Biology, Cornell University, Ithaca, NY, 14853, United States

ARTICLE INFO

Article history:
Received 24 April 2015
Received in revised form
11 May 2015
Accepted 21 May 2015
Available online 30 May 2015

Keywords:
Ammine ligand
Tetrahedral coordination
π-type interaction
Energy resonance
Valence-to-core emission

ABSTRACT

A detailed orbital analysis of two seemingly ordinary classes of complexes of group 12 dications, $[M(NH_3)_4]^{2+}$ and $[M(PH_3)_4]^{2+}$, M = Zn, Cd, Hg, holds a surprise. The PH_3 complexes are text-book examples of tetrahedral bonding, but in the ammine complexes calculations reveal a remarkable degree of mixing between occupied M *(n-1)d* and NH_3 σ_π orbitals. A perturbation-based Fock matrix examination traces the origin of this mixing to an energy resonance and improved overlap of interacting orbitals for NH_3 ligands. The possibility of probing this anomalous mixing with valence-to-core X-ray emission spectroscopy (V2C XES) is discussed.

1. Introduction

In the course of searching for an inverted ligand-field splitting [1], we had occasion to look at the electronic structure of a seemingly normal series of Group 12 M(II) complexes — $[M(EH_3)_4]^{2+}$, E = N, P, As, Sb, Bi; M = Zn, Cd, Hg. Phosphine (PH_3) complexes are uncommon, but PR_3 ligands are a workhorse of coordination and organometallic chemistry [2–6]. The ammine (NH_3) complexes are common, especially the Zn ones, and a typical structure of these complexes is shown in Fig. 1. The orbital mixing in these $[M(NH_3)_4]^{2+}$ ions, however, turns out, as we will see, to be atypical.

Usually, EH_3, E = Group 15 elements, are considered classic Lewis bases: σ-donor ligands that bond with metals primarily through high-lying lone-pair orbitals localized on the E atom. In a 4-coordinate complex with rigorous T_d symmetry, the lone pairs generate symmetry-adapted $a_1 + t_2$ orbital combinations. These then interact with metal orbitals of the same symmetry and induce t_2-*e* splitting, leaving the *e*-type *(n-1)d* orbitals as noninteracting orbitals (see Fig. 2) [7]. As Landis and Weinhold have pointed out [8], the contribution of the metal *np* orbitals to the two low-lying t_2 levels is small.

EH_3 ligands are not thought to engage in π-bonding, but a detailed orbital analysis in this work suggests reconsideration of this perspective, at least for some E. In addition to the lone pair on E, the EH_3 ligands contain three delocalized E-H bonding orbitals, shown in Fig. 3 for NH_3, with $a_1 + e$ symmetry in the C_{3v} point group of the ligand, and a set of corresponding E-H antibonding orbitals. The *e* combination, containing N $2p_{x/y}$, has π symmetry, so we will call the orbital set σ_π; in contrast, the a_1 combination contains N *2s* and $2p_z$ and we call it σ_σ. In these two labels, the inline σ indicates the N–H bond type, while the subscripts σ *and* π characterize the symmetry of the orbitals with respect to N–M bonding when NH_3 serves as a ligand.

In the T_d point group of the $[M(EH_3)_4]^{2+}$ ions, the eight σ_π orbitals combine to form *e*, t_1, and t_2 symmetry-adapted orbitals. Five (*e*, t_2) of the eight can interact with the valence *d*-orbitals of the metal, in the standard π-bonding picture of tetrahedral complexes familiar to the community for 50 years [9]. While π-type metal-ligand bonding is important for π-acceptors such as CO, CN^-, and PF_3, and for π-donors such as O^{2-}, Cl^-, and SR, neither NH_3 nor PH_3 are recognized as particularly good π-donor or acceptor ligands. The E-H bonding orbitals are thought to be too low in energy to interact with the valence *d*-orbitals of the metal. We examine the validity of these ideas with detailed calculations.

2. The expected behavior of phosphine ligands

The traditional orbital mixing picture outlined above proves correct for the $[M(PH_3)_4]^{2+}$ series. The highest-lying occupied molecular orbital (MO) energies are shown in Table 1. Also shown are the results of a Natural Population Analysis (NPA) [10] that

☆ One can just feel the desire to understand inorganic molecules in Mike Mingos' work. Thank you for this gift to all of us.

* Corresponding author.
E-mail address: rh34@cornell.edu (R. Hoffmann).

http://dx.doi.org/10.1016/j.jorganchem.2015.05.032
0022-328X/

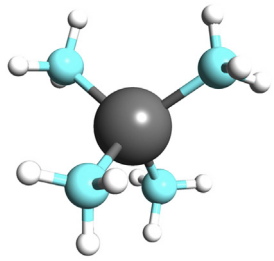

Fig. 1. $[Zn(NH_3)_4]^{2+}$.

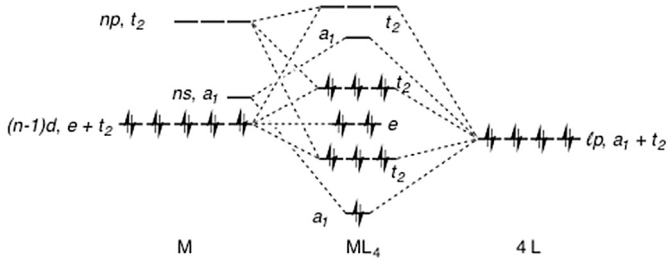

Fig. 2. Typical orbital interaction diagram for d^{10} tetrahedral ML_4 complexes. Here "*lp*" stands for lone-pair orbitals of the ligands.

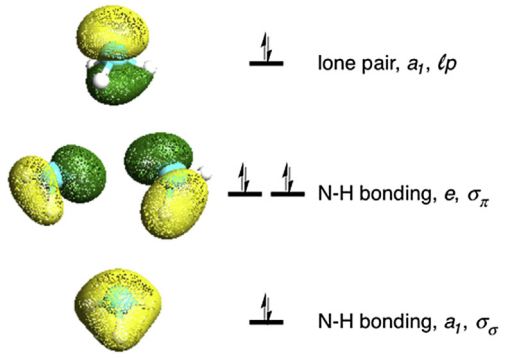

Fig. 3. The valence occupied orbitals of NH_3, their irreducible representations, and the labels (*lp*, σ_π, and σ_σ) used in the discussions below.

describes the composition of the molecular orbitals (MOs) as percentage contributions from the metal (M%) and the four ligands' (4L %) orbitals. We use DFT with the M06 functional to generate the results reported here, and provide additional details of calculations in the Theoretical Methods section at the end of the paper. The low orbital energies stem from the +2 charge of the ionic complexes. We probed the effect of the overall charge by calculations on a neutral $[Zn(PH_3)_4](BF_4)_2$ molecule. As expected, the orbital energies increase, but the orbital character remains essentially unchanged.

Table 1 includes a larger number of interacting orbitals than are shown in Fig. 2. The corresponding modified version of the interaction diagram that includes the σ_π orbitals of the ligands is shown in Fig. 4. Note that in this diagram, the metal orbital energies are lowered to reflect the +2 charge concentrated on the electropositive metal center.

ML_4 bonding occurs mainly through the a_1 MO, a bonding combination of the M *ns* and the PH_3 lone pairs with 35:65, 33:67, and 26:74 M:4L mixing in the three phosphine ions. The t_2 highest occupied MO (HOMO) is less involved in bonding, and has contributions mainly from the ligand lone pairs, with a small admixture (4–7%) of M *np* (with bonding character) and *(n-1)d* (with antibonding character).

Table 1
Energies of the highest lying occupied orbitals of the three Group 12 dication phosphine complexes listed in the first column, and the percentage populations on the metals (M%) and the four ligands (4L%) in each orbital from NPA. The approximate character of each orbital is specified in the last column with "*ab*" standing for antibonding, "*b*" for bonding, "*ni*" for noninteracting, "*lp*" for lone-pair on the ligand, and "σ_π" for the π-like P–H bonding orbital in the PH_3 ligands. The "*s*", "*p*", and "*d*" symbols indicate the type of metal valence orbital.

	Orbital	E/eV	M%	4L%	Character
$[Zn(PH_3)_4]^{2+}$	t_2	−16.63	4	96	*lp-4p b*
	t_1	−19.35	0	100	σ_π *ni*
	e	−19.54	1	99	σ_π *ni*
	t_2	−19.57	0	100	σ_π *ni*
	a_1	−19.67	35	65	*lp-4s b*
	e	−22.97	99	1	*3d ni*
	t_2	−23.02	96	4	*3d ni*
$[Cd(PH_3)_4]^{2+}$	t_2	−16.37	4	96	*lp-5p b*
	a_1	−18.99	33	67	*lp-5s b*
	t_1	−19.17	0	100	σ_π *ni*
	e	−19.29	1	99	σ_π *ni*
	t_2	−19.32	0	100	σ_π *ni*
	e	−23.78	99	1	*4d ni*
	t_2	−23.81	93	7	*4d ni*
$[Hg(PH_3)_4]^{2+}$	t_2	−16.02	7	93	*lp-5d ab/lp-6p b*
	t_1	−19.12	0	100	σ_π *ni*
	e	−19.14	4	96	σ_π *ni*
	t_2	−19.22	0	100	σ_π *ni*
	a_1	−19.23	26	74	*lp-6s b*
	e	−21.53	96	4	*5d ni*
	t_2	−21.67	92	8	weak *lp-5d b*

It is clear from Table 1 that the PH_3 σ_π orbitals are largely unchanged from the individual ligand orbitals. We label these orbitals noninteracting (*ni*). The *ni*, $t_1 + t_2 + e$, σ_π set is never split by more than 0.22 eV, and is 96–100% localized on the four ligands for the Group 12 dication series.

To summarize, the orbitals of $[M(PH_3)_4]^{2+}$ are textbook — dative bonding to the metal is largely through the phosphine lone pairs, and the PH_3 σ_π orbitals do not engage in π-bonding. We also calculate the structure of the phosphine ion complexes and find some interesting features; these are discussed in a separate section below.

3. The unusual behavior of ammine ligands

Having set the stage with the PH_3 ligand, one can appreciate our surprise when we investigated the nature of bonding for a similarly "normal" ligand, ammonia. Table 2 shows our calculated results for orbital energies and compositions in $[M(NH_3)_4]^{2+}$, M = Zn, Cd, Hg. Like the phosphine complexes, the geometrical structures of

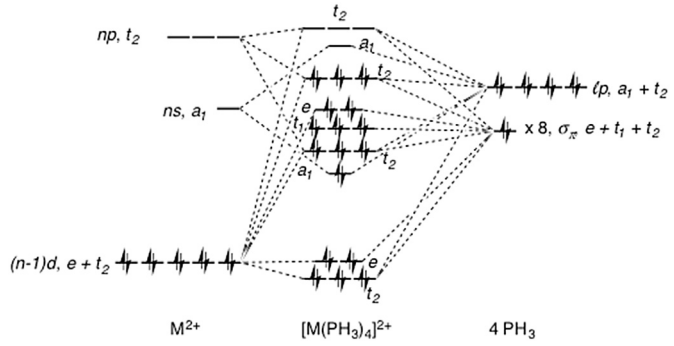

Fig. 4. Schematic orbital interaction diagram for $[M(PH_3)_4]^{2+}$. The a_1, t_2, *e*, and t_1 levels in the $[M(PH_3)_4]^{2+}$ ranging from 3rd to 6th in increasing order of energy are close in energy (Table 1) and their relative positions in this schematic diagram do not represent their actual energy ordering.

Table 2
Energies of the highest lying occupied orbitals of the three Group 12 dication ammine complexes listed in the first column, and the percentage populations on the metals (M%)and ligands (4L%) in each orbital from NPA. The character of each orbital is specified in the last column with "*ab*" standing for antibonding, "*b*" for bonding, "*ni*" for noninteracting, "*lp*" for lone-pair on the ligand, "σ_π" for the π-like N–H bonding orbital in the NH_3 ligands. The "*s*", "*p*", and "*d*" symbols indicate the type of metal valence orbitals.

	Orbital	E/eV	M%	4L%	Character
$[Zn(NH_3)_4]^{2+}$	t_2	−18.58	12	88	*lp-4p b/lp-3d ab*
	a_1	−21.43	20	80	*lp-4s b*
	e	−21.98	59	41	σ_π*-3d ab*
	t_1	−22.52	0	100	σ_π *ni*
	t_2	−22.61	30	70	σ_π*-3d ab*
	t_2	−23.19	58	42	σ_π*-3d b/lp-3d b*
	e	−23.36	41	59	σ_π*-3d b*
$[Cd(NH_3)_4]^{2+}$	t_2	−18.09	10	90	*lp-5p b/lp-4d ab*
	a_1	−20.50	19	81	*lp-5s b*
	e	−22.02	23	77	σ_π*-4d ab*
	t_1	−22.28	0	100	σ_π *ni*
	t_2	−22.37	4	96	σ_π*-4d ab*
	e	−23.82	77	23	σ_π*-4d b*
	t_2	−23.87	85	15	σ_π*-4d b/lp-4d b*
$[Hg(NH_3)_4]^{2+}$	t_2	−17.57	18	82	*lp-6p b/lp-5d ab*
	a_1	−20.47	13	87	*lp-6s b*
	e	−20.98	77	23	σ_π*-5d ab*
	t_2	−21.78	60	40	σ_π*-5d ab*
	t_1	−22.20	0	100	σ_π *ni*
	t_2	−22.49	22	78	σ_π*-5d b/lp-5d b*
	e	−22.70	23	77	σ_π*-5d b*

ammine complexes are also calculated and will be discussed below.

The calculated MOs involving σ_π in the three tetraammine dication complexes are far from pure ligand or pure metal. As Table 2 shows, the high-lying *e* orbitals have M:4L mixings of 59:41, 23:77, and 77:23, definitely more substantial than those listed in Table 1. Their low-lying counterparts, which in the phosphine cases were pure metal *(n-1)d*, have complementary mixings of 41:59, 77:23, and 23:77. These pronounced orbital mixings point to unexpected π-interaction in the ammine complexes.

4. The origin of σ_π and *(n-1)d* mixing in ammine complexes

We start by investigating the normal behavior of the phosphine ions and the absence of σ_π*-(n-1)d* interaction in Table 1. We focus on the *e*-irreducible representation of the T_d point group that involves mixing *(n-1)d* and linear combinations of the σ_π orbitals, since this interaction between *e*-type orbitals is not contaminated by the interactions with *lp-(n-1)d* and *lp-ns*. In the upper half of Table 3 we present the diagonal and off-diagonal matrix elements of the Fock operators of the σ_π and *(n-1)d* orbitals of $[M(PH_3)_4]^{2+}$ at their optimized structures. The Coulomb and exchange operators within the Fock operator are constructed using the occupied MOs from the converged DFT calculations of the respective ions. The diagonal elements indicate the orbital energies in the environment of the ion complexes and the off-diagonal elements gage the interaction strength between the orbitals.

The σ_π and *(n-1)d* orbitals are obtained from calculations of neutral $(PH_3)_4$ and metal atoms, with the four PH_3 retaining the geometries of the respective $[M(PH_3)_4]^{2+}$ ions. The σ_π and *(n-1)d* are thus not orthogonal, and their overlap integrals, that are approximately proportional to the off-diagonal Fock matrix elements and reflect the interaction strength, are also reported in Table 3.

It is interesting to note that the overlap and off-diagonal matrix elements roughly satisfy the Wolfsberg–Helmholz relation: [11]

$$F_{d,\sigma_\pi} = KS_{d,\sigma_\pi}\frac{F_d + F_{\sigma_\pi}}{2},$$

with *K* ranging from 1.36 to 1.43 for the phosphine (1.43 to 1.50 for the ammine) ions. The proportionality of the off-diagonal Hamiltonian matrix element to the overlap is also at the heart of the extended Hückel theory [12], a method that has served one of the authors well over the years.

The *e* MO energies and NPA results obtained within this contracted orbital space are in quantitative agreement with those obtained from the fully optimized electronic structure results in Table 1, and serve to demonstrate the adequacy of this orbital space.

The *(n-1)*d and σ_π energies (F_d and F_{σ_π}) in the upper half of Table 3 differ by more than 2.3 eV, with the *(n-1)d* being lower. These significant energy gaps impede σ_π*-(n-1)d* interactions. The F_{d,σ_π} coupling elements are of the order of −1 eV, and are seemingly large enough to couple the *(n-1)d* and σ_π orbitals, despite the energy gap. However, recall that the interacting orbitals are normalized but non-orthogonal, making F_{d,σ_π} an overestimated coupling. The effective coupling matrix is, then, $\underline{F} - \underline{S}E_{MO}$ [13]. For instance, in $[Zn(PH_3)_4]^{2+}$, $F_{d,\sigma_\pi} - S_{d,\sigma_\pi}E_{MO} = -0.24$ and −0.35 eV for the two E_{MO} values. The magnitude of the effective coupling is insufficient to overcome the >2.3 eV σ_π*-(n-1)d* energy gaps, resulting in relatively pure σ_π and *(n-1)d* orbitals in the phosphine ion complexes.

Completing our discussion of the "normal" phosphine ions, we note that $[Hg(PH_3)_4]^{2+}$ is anomalous within this series. Among the three phosphine ion complexes, it has the smallest σ_π*-(n-1)d* gap and the largest coupling between the two orbitals. Correspondingly, it features the "largest" σ_π*-(n-1)d* mixing, reflected by the 4% (0.08 electron) Natural Population transfer between the two orbitals. The diminished gap arises from the higher *5d* energy of Hg relative to the *4d* and *3d* of Cd and Zn (−21.49 *vs.* −23.75 and −22.94 eV), a manifestation of the relativistic *d* expansion [14,15]. This expansion of Hg *5d* also favors the σ_π*-(n-1)d* π-type overlap and leads to the maximum overlap (0.054, Hg, *vs.* 0.043, Cd, and 0.032, Zn) and coupling (−1.49 *vs.* −1.29 and −0.97 eV) in the series under discussion. Despite this, the relativistic anomaly here is not large enough to substantially mix the σ_π and *5d*.

Turning now to the ammines and their noticeable σ_π*-(n-1)d* mixing, a similar analysis can be used to explain the mixings seen in Table 2 for $[M(NH_3)_4]^{2+}$. The Fock matrix elements are calculated and reported in the lower half of Table 3. The NH_3 σ_π orbitals lie lower in energy than those of PH_3, about −22 vs −19 eV in the respective families of ions. This is consistent with the electronegativities of N and P — the σ_π energy in free NH_3 is lower than that in free PH_3 (−12.68 vs −10.68 eV). The lower-lying NH_3 σ_π orbitals are closer in energy to the metal *d* orbitals, with a maximum gap of 1.08 eV for $[Cd(NH_3)_4]^{2+}$. This makes the σ_π*-(n-1)d* interaction stronger than in the phosphine complexes.

In Fig. 5, we show schematically the orbital interaction of

Table 3
Matrix elements of the $[M(PH_3)_4]^{2+}$ and $[M(NH_3)_4]^{2+}$ Fock operators between the metal *(n-1)d* orbitals and ligand σ_π orbital-combinations that transform as the *e* irreducible representation of the T_d point group (F_d and F_{σ_π}, diagonal; F_{d,σ_π}, off-diagonal), their overlap integrals (S_{d,σ_π}), the resultant molecular orbital energies (E_{MO}) obtained from diagonalizing the 2 × 2 Fock matrix, and the Natural Population of the low-lying MO on the metals (M%).[a] All energy quantities are in the unit of eV.

	F_d	F_{σ_π}	F_{d,σ_π}	S_{d,σ_π}	E_{MO}	M%
$[Zn(PH_3)_4]^{2+}$	−22.94	−19.51	−0.97	0.032	−22.95, −19.48	99
$[Cd(PH_3)_4]^{2+}$	−23.75	−19.29	−1.29	0.043	−23.76, −19.24	99
$Hg(PH_3)_4]^{2+}$	−21.49	−19.20	−1.49	0.054	−21.49, −19.10	96
$[Zn(NH_3)_4]^{2+}$	−22.60	−22.72	−2.00	0.059	−23.28, −21.96	44
$[Cd(NH_3)_4]^{2+}$	−23.47	−22.39	−2.27	0.068	−23.78, −21.79	79
$[Hg(NH_3)_4]^{2+}$	−21.44	−22.25	−2.37	0.076	−22.61, −20.97	24

[a] Showing M% for one MO suffices, as M% and 4L% add up to 100 in one orbital and the M:4L composition in the higher-lying orbital is reversed to the low-lying one.

$[M(NH_3)_4]^{2+}$. The origin of the unexpected orbital mixing observed in the ammine complexes is, clearly, due to the significantly smaller separation in energy of the σ_π and *(n-1)d* orbitals.

Besides the smaller σ_π-*(n-1)d* energy gap, the σ_π-*(n-1)d* couplings and overlaps are more substantial in the ammine than in the phosphine ion complexes. This is attributed to the general finding [16,17] that *p*-block elements other than those of the second period have low propensity for π-type overlap, π-bonding in general. Both the smaller gap and the larger couplings shape the pronounced σ_π-*(n-1)d* mixings of $[M(NH_3)_4]^{2+}$ shown in Table 2.

The variable extent of σ_π-*(n-1)d* mixing in the three ammine ion complexes merits further examination. The mixing is reduced from $[Zn(NH_3)_4]^{2+}$ (41:59) to $[Cd(NH_3)_4]^{2+}$ (77:23), because the lowering of the *d* orbital energy from Zn to Cd increases its energy "distance" (from 0.12 higher than to 1.08 eV lower than σ_π) from the NH_3 σ_π orbitals. This *d* energy-lowering is also reflected by the increase of metal contribution in the lower *e* MO from 41% to 77%. For $[Hg(NH_3)_4]^{2+}$, the relativistic *5d* expansion[14,15] raises the *5d* energy 0.81 eV higher than that of the σ_π; it reduces the metal contribution in the lower *e* MO to 23%. The nearly degenerate *3d* and σ_π orbitals make for the most pronounced σ_π-*(n-1)d* mixing in $[Zn(NH_3)_4]^{2+}$. Fig. 6 shows the one component of the degenerate bonding (a) and antibonding (b) *e* orbitals in $[Zn(NH_3)_4]^{2+}$; note how "covalent" they appear.

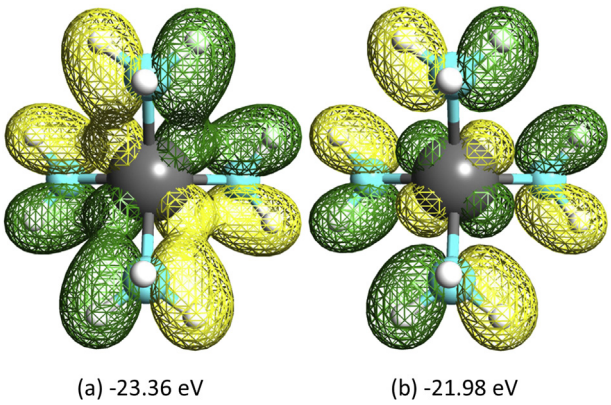

Fig. 6. The two *e* occupied MOs in $[Zn(NH_3)_4]^{2+}$ with their energies shown below them.

5. Can the anomalous orbital mixing be observed?

The σ_π-*(n-1)d* mixing in the *e* MOs of $[M(NH_3)_4]^{2+}$ does not affect bond strengths or geometries. Any bonding effects due to the low-energy *e* MO are counteracted by the antibonding effects of the high-energy *e* MO, as they are both occupied. In other words, the bonding and antibonding *e* MOs, not that different in energy, may be recombined to form pure, noninteracting metal *d* orbitals and ligand σ_π orbitals, leaving the Kohn-Sham determinant and the electron density of the complex ion unchanged.

Still, the mixing is substantial in the canonical orbitals. Can it be observed experimentally? Valence-to-core X-ray emission spectroscopy (V2C XES) provides, in principle, a way [18–21]. When X-ray photoionization generates a hole in one of the core orbitals of the metal, *2p* say, both the electrons from either bonding or antibonding *e* MOs can fill the hole by energetically demoting with concomitant photon ejection. Since the donor orbitals in these cases both have significant metal *d* contributions, substantial transition dipole moments follow. Two distinguishable *e*-to-core transitions in V2C XES would strongly support the σ_π-*(n-1)d* mixing. Complications from splitting of M *2p* by spin–orbit coupling (SOC) can be mitigated by photoexcitation at energies between the well-separated $2p_{1/2}$ (L_2) and $2p_{3/2}$ (L_3) edges, yielding a state with a principally $2p_{3/2}$ core hole.

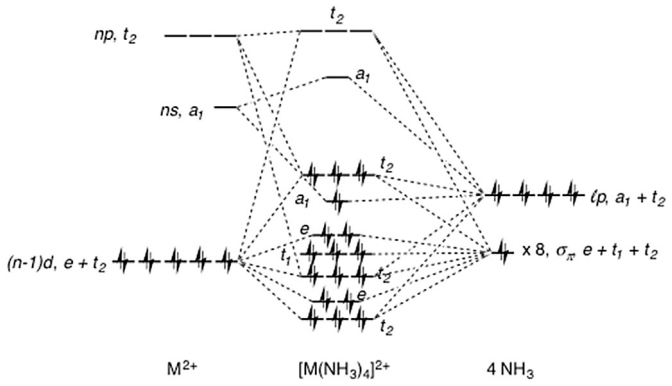

Fig. 5. Schematic orbital interaction diagram for $[M(NH_3)_4]^{2+}$. The lowest *e* and t_2 levels (t_1 and the second lowest t_2 also) are close in energy (Table 2) and their relative positions in this schematic diagram do not represent their actal energy ordering.

We note that the energy splitting between the two *e* MOs does not exceed 1.8 eV in Table 2 for the three ammine ions. Given current technical limitations, such a modest splitting will be difficult to resolve in V2C XES measurements. Also, distinguishing between *e*-to-core transitions and the close-lying t_2-to-core transitions may prove challenging. This is especially true for $[Hg(NH_3)_4]^{2+}$, where substantial spin–orbit coupling (SOC) mixes the *e* and t_2 MOs.

However, it is not necessary that we constrain ourselves to the two *e* MOs. The σ_π-*(n-1)d* mixing occurs in t_2 MOs as well. Overall, these orbital mixings, regardless whether in *e* or t_2 MOs, leads to a broader distribution of *d* contributions in MOs and therefore, broader valence-to-$2p_{3/2}$ transitions.

To elaborate on this idea, we calculate the valence-to-$2p_{3/2}$ emission spectra for the ammine and phosphine ions, shown in Fig. 7 (Figs. S1 and S2 in the Supporting Information provide the decompositions of the transition profiles to the constituent transitions). As expected, the main transition peaks corresponding to the *e*- and t_2-to-$2p_{3/2}$ transitions are significantly broader for $[M(NH_3)_4]^{2+}$ than for $[M(PH_3)_4]^{2+}$.

The details of the spectra warrant further discussion. The main peak in the $[Cd(NH_3)_4]^{2+}$ spectrum stems from the σ_π-*(n-1)d* bonding orbitals with lower transition energy (around 3530 eV), while the shoulder between 3532 and 3533 eV arises from σ_π-*(n-1)d* antibonding orbitals. This is because the bonding orbitals have larger contributions from Cd *4d* than the antibonding ones. The situation is reversed in the $[Hg(NH_3)_4]^{2+}$ spectrum; the main peak at 12315 eV corresponds to antibonding orbitals, while the lower energy shoulder corresponds to bonding orbitals. As mentioned above, the Hg *5d* contributes more to the antibonding orbitals due to its relativistic expansion.

For $[Zn(NH_3)_4]^{2+}$, although the bonding *e* MO has less metal contribution (41:59, Table 2) than the antibonding *e*, the adjacent bonding t_2 MO has more metal contribution (58:42, Table 2) than the antibonding t_2. The three-fold degeneracy of the t_2 MO versus the two-fold degeneracy of the *e* MO make the former more dominant and places the main peak at a lower energy of 1006 eV, which corresponds to the bonding MO, with the antibonding shoulder at 1007 eV. The shoulder is not much lower than the main peak intensity, reflecting the fairly balanced metal and ligand distributions in the bonding and antibonding MOs.

Within the phosphine ions, $[Hg(PH_3)_4]^{2+}$ contains more σ_π-*(n-1)d* mixing (Table 1) than the other two and it features the broadest

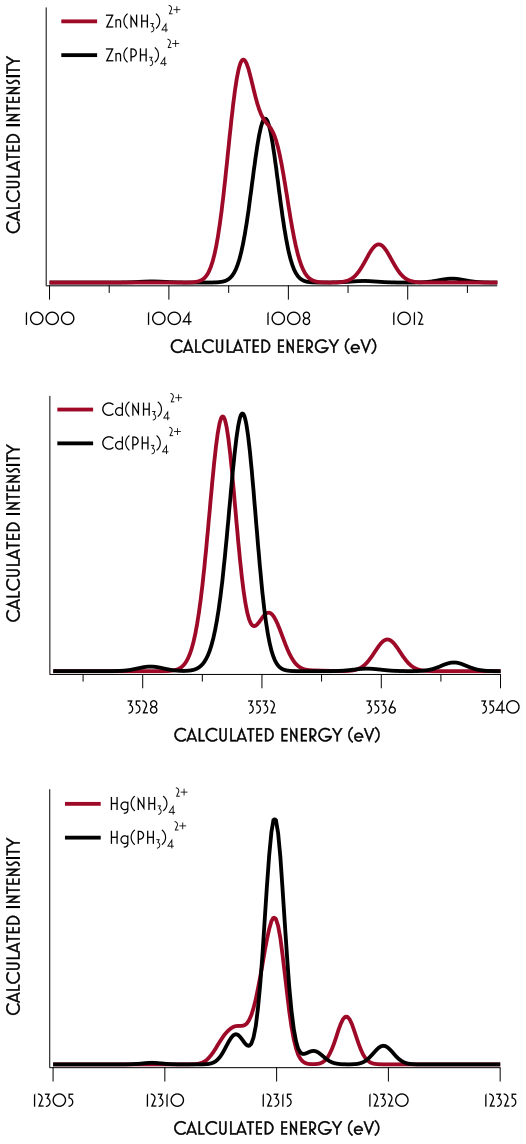

Fig. 7. DFT (M06/def-TZVP-ZORA + SOC) calculated V2C XES (Valence → $2p_{3/2}$) of all $[M(NH_3)_4]^{2+}$ and $[M(PH_3)_4]^{2+}$ (M = Zn, Cd, Hg) ions. In this figure we compare the different transition profiles of the ammine and phosphine complexes. Please refer to Figs. S1 and S2 in the Supporting Information for the detailed description of the transitions.

distribution of valence-to-$2p_{3/2}$ transitions. It is noteworthy that the little peaks at the highest energy arise from HOMO t_2-to-$2p_{3/2}$ transitions, reflecting the magnitude of *lp-(n-1)d* antibonding mixing. Although those transitions are more pronounced in ammine than in phosphine ions, they should not be considered evidence of σ_π-*(n-1)d* mixing.

Overall, the differences between the ammine and phosphine ions in the calculated valence-to-$2p_{3/2}$ emission spectra are obvious and should be discernable in real spectra. The anomalous σ_π-*(n-1)d* mixing in the ammine ions is an observable phenomenon.

6. Structures: an intriguing bond angle effect

Table 4 summarizes the calculated geometries of the $[M(PH_3)_4]^{2+}$ complexes. No direct experimental information is available for comparison, as the complexes have apparently not been synthesized, possibly due to the inflammability, toxicity, and explosiveness of PH_3 [22]. However, M–P distances are available for other PR_3 ligands in the coordination sphere of Zn and Hg, and our calculated bond lengths deviate from them by about 0.1 Å, generally satisfactory agreement.

For PH_3, there is a significant opening up of the H–P–H angle from 93 to 102° in the complexes. This seemingly "counter-steric" trend is interesting and is explained as follows: to form a stronger dative bond with M^{2+}, the PH_3 lone pair requires more *3p* character, so as to "protrude" more towards the metal. The hybridization change is in accordance with Bent's rule [24] that a *p*-block atom's hybrid orbital directed towards an electronegative atom carries more *p* character; the metal dication "ligand" is highly electronegative.

Correspondingly, we expect less P *3p* character in the PH bond pairs. Indeed, the *s*:*p* character ratio in the P hybrid of the PH bond pair natural bond orbital [10] (NBO) changes from 15:85 in the free molecule to about 25:75 in the $[M(PH_3)_4]^{2+}$ complexes. This reduction of *p* character in the hybrids opens up the angles between them (recalling the 109.5° of C sp^3 hybrids, 120° of C sp^2 hybrids, and 180° of C *sp* hybrids), and the 102° H–P–H angle in the ions is close to the 109.5° of the ideal sp^3 hybridization limit. The wider H–P–H angle is thus a result of the rehybridizing P in the ion complexes.

The R-P-R angle also widens upon coordination; a flattening of the PR_3 ligand, is observed experimentally in $Zn(PMe_3)_4^{2+}$. The C–P–C angle is 98.6° in the free PMe_3 molecule [25] but widens to 105° in $Zn(PMe_3)_4^{2+}$ [23]. The 105° C–P–C angle compares well with the 102° of our calculated H–P–H angles, reflecting the accuracy of our methodology. Note that the 105° C–P–C angle has little to do with the steric repulsion between the methyls attached to the same P, as the shortest distance between H atoms on different methyls is 2.7 Å, greater than twice of H's van der Waals radius (1.2 Å) [26]. In addition, any methyl–methyl steric effect would have been observed in the free PMe_3 molecule. The change in PR_3 pyramidalization on coordination, slight as it is, has some implications for the important Tolman cone angles, so useful in making sense of steric effects of ligands [27,28].

Unlike the case of $[M(PH_3)_4]^{2+}$, the literature contains several of structurally characterized $[M(NH_3)_4]^{2+}$ for Group 12 metals. Our calculated structures are as expected and agree well with experiment (Table 5). The calculated Zn–N and Hg–N distances deviate from experimental values by less than 0.1 Å. We have found no

Table 4
Optimized structural parameters for $[M(PH_3)_4]^{2+}$: M–P bond length ($R_{M\text{-}P}$), P–H bond length ($R_{P\text{-}H}$), and H–P–H bond angle ($\angle_{H-P-H}$). Experimental $R_{M\text{-}P}$ for substituted M $(PR_3)_4^{2+}$ are provided under the calculated ones for comparison.

	$R_{M\text{-}P}$/Å	$R_{P\text{-}H}$/Å	$\angle_{H-P-H}$/°
$[Zn(PH_3)_4]^{2+}$	2.424	1.403	101.9
	2.370–2.390[a]		105[a]
$[Cd(PH_3)_4]^{2+}$	2.565	1.403	101.5
$[Hg(PH_3)_4]^{2+}$	2.655	1.404	102.1
	2.527–2.547[b]		
	2.552–2.585[c]		
	2.512–2.613[d]		
Free PH_3		1.418	93.3
		1.4200[e]	93.345[e]

[a] Experimental Zn–P bond length and C–P–C angle for $[Zn(PMe_3)_4][BAr^F_4]_2$ taken from Ref. [2]. $BAr^F_4 = B\{C_6H_3(CF_3)_2\}_4$. The C–P–C angle is to compared with the H–P–H angle.

[b] Experimental Hg–P bond length for $[Hg(PMe_2Ph)_4][Ta_2OCl_{10}]$ taken from Ref. [4].

[c] Experimental Hg–P bond length for $[Hg(7,8\text{-}(PPh_2)_2\text{-}7,8\text{-}C_2B_9H_{10})_2]CH_2Cl_2$ taken from Ref. [5].

[d] Experimental Hg–P bond length for $Hg(dppe)_2^{2+}$ taken from Ref. [6]. dppe = $Ph_2PCH_2CH_2PPh_2$.

[e] Experimental P–H bond length and H–P–H bond angle for PH_3[23].

Table 5
Optimized structural parameters for $[M(NH_3)_4]^{2+}$: M–N bond length (R_{M-N}), N–H bond length (R_{N-H}), and H–N–H bond angle ($\angle_{H-N-H}$). Experimental R_{M-N} are provided under the calculated ones for comparison.

	R_{M-N}/Å	R_{N-H}/Å	$\angle_{H-N-H}$/°
$[Zn(NH_3)_4]^{2+}$	2.042	1.018	104.7
	2.05[a]		
	1.997–2.030[b]		
$[Cd(NH_3)_4]^{2+}$	2.202	1.017	105.1
$[Hg(NH_3)_4]^{2+}$	2.331	1.016	106.1
	2.247–2.281[c]		
Free NH_3		1.020	105.4
		1.012[d]	106.67[d]

[a] Experimental Zn–N bond length for $[Zn(NH_3)_4]Mo(O_2)_4$ [29].
[b] Experimental Zn–N bond length for $[Zn(NH_3)_4]I_2$ [30].
[c] Experimental Hg–N bond length for $[Hg(NH_3)_4](ClO_4)_2$ [31].
[d] Experimental NH_3 bond length and bond angle [32].

neutron diffraction structures to give us reliable experimental NH distances, but for free NH_3, the theory-experiment agreement is excellent. Unlike the case of $[M(PH_3)_4]^{2+}$, the H–N–H angle of the NH_3 ligand is similar to that of the free molecule. The NH_3 lone pair has high enough p character (75% in the NH_3 NBO lone pair, *vs.* 43% in the PH_3 counterpart) to form a strong M–N dative bond and there is no need for the rehybridization that widens the H–P–H angle in the PH_3 ligand.

Hessian calculations at the optimized structures found no imaginary frequencies, except for $[Cd(NH_3)_4)]^{2+}$ and $[Cd(PH_3)_4)]^{2+}$. The $[Cd(NH_3)_4]^{2+}$ ion departed from the ideal tetrahedron, along an *e* twisting mode. This deformation would eventually take it to square-planar coordination, but the degree of distortion, to N–Cd–N angles of 93° and 119° and no change in bond lengths, is not great. And the energy gain is small, 0.09 eV. Sterically driven distortion of $[M(NR_3)_4]^{2+}$ or $[M(PR_3)_4]^{2+}$ are common, but an ammine ligand is unlikely to provoke this, so the effect is probably electronic. Most $[CdR_4]^{2+}$ structures show a close to tetrahedral geometry. An unusual $Cd(OR)_2(THF)_2$ compound is square-planar at Cd [33], but the Cd–O(THF) distances are long, so that the molecule is close to a 2-coordinated Cd(II) complex with weakly coordinated bases.

The kinetics and mechanism of stereoisomerization of bis–bidentate complexes of Zn(II) and Cd(II) (and other ions) have been carefully studied by Minkin, Nivorozhkin, Korobov, and their coworkers [34]. A variety of mechanisms was observed, including dissociation-recombination, associative, and intramolecular stereoiosmerization. Cd(II) offers some carefully worked out examples of the last, the intramolecular process, with relatively low barriers [37].

We judge the distortion calculated for $[Cd(NH_3)_4]^{2+}$ to be weak, and the discussion of orbital mixing above for $[Cd(NH_3)_4]^{2+}$ is based on its tetrahedral structure. Similar e-type imaginary frequencies are also obtained for $[Cd(PH_3)_4]^{2+}$. However, geometry optimization starting with a distorted D_{2d} structure returns directly to a T_d structure. It is clear that the potential energy surface for deformation of these complexes from tetrahedral geometry is quite flat.

7. Conclusions

NH_3 is considered a typical Lewis base ligand, acting mainly through its lone pair electrons. However, the present theoretical study shows unexpected π-bonding/antibonding interaction involving the NH σ_π bonding orbitals in $[M(NH_3)_4]^{2+}$ cationic complexes with Group 12 metal centers Zn, Cd, and Hg. The interaction between the π-type NH σ_π orbitals and the metal centers' valence *d* orbitals are shown to stem from the small energy gap between them in the cationic system. In contrast, the PH bond pairs in PH_3 are energetically well separated from the metal *d* orbitals, and our calculations show no interesting interactions.

The interaction we observe computationally has little effect on the geometries of the compounds. Yet it is striking and surprising. We discuss the possibility of using V2C XES to experimentally observe the σ_π-*(n-1)d* mixing. The broadening of valence-to-$2p_{3/2}$ transitions in the $[M(NH_3)_4]^{2+}$ spectra, compared to the sharp transitions in the $[M(PH_3)_4]^{2+}$ spectra, may serve as evidence for the mixing. Devising further experiments to observe the anomalous orbital mixing we uncovered is an interesting subject for future research.

8. Theoretical methods

Density function theory (DFT) calculations using the M06 [35] functional and the SPK-TZP [36–45] basis sets were carried out to optimize the structures of all phosphine and ammine ions with center metals Zn and Cd and obtain their orbitals. For the ions with Hg center, the SARC-DKH [46] basis set is used for Hg and cc-pVTZ [47] basis sets are used for nonmetal atoms. The third order Douglas-Kroll Hamiltonian [48,49] is used to treat the relativistic effects. The convergence criteria for self-consistent field iteration and geometry optimization are 10^{-6} and 10^{-5} a.u., respectively. In the calculations of the V2C XES in Fig. 7, the def2-TZVP-ZORA basis sets [50] are used, and the associated two-component Hamiltonian handles the spin–orbit coupling explicitly. All calculations except for the V2C spectra were done using the GAMESS-US [51,52] quantum chemistry program package. The V2C spectra are obtained using ORCA [53]. Gaussian functions with 1 eV full width at half maximum (FWHM) are used to broaden the calculated transition spikes shown in Figs. S1 and S2 in the Supporting Information to the transition profiles shown in Fig. 7.

Acknowledgments

T.Z. thanks the Natural Sciences and Engineering Research Council of Canada for the Banting postdoctoral fellowship (201211BAF-303459-236530). R.H. is grateful to the National Science Foundation for its support of this work though Grant CHE-1305872. K.M.L gratefully acknowledges the Cornell University College of Arts and Sciences for startup funding. N. A. acknowledges Cornell Start-up funding. We thank Frank Weinhold for providing us with the NBO6.0 program package. T.Z. is grateful to Mike Schmidt and Mark Gordon for their continuous support of the GAMESS-US program package.

Appendix A. Supplementary data

Supplementary data related to this article can be found at http://dx.doi.org/10.1016/j.jorganchem.2015.05.032.

References

[1] T. Zeng, T.J. Cahill, S. Alvarez, C. Mealli, R. Hoffmann, to be published.
[2] H. Banh, C. Gemel, R.W. Seidel, R.A. Fischer, Chem. Comm. 51 (2015) 2170–2172.
[3] D.A. Dickie, R.A. Kemp, Organometallics 33 (2014) 6511–6518.
[4] F.A. Cotton, S.A. Duraj, W.J. Roth, Acta Cryst. C41 (1985) 881–883.
[5] L. Kong, D. Zhang, F. Su, D. Li, J. Dou, Bull. Korean Chem. Soc. 32 (2011) 2249–2252.
[6] F. Cecconi, C.A. Ghilardi, P. Innocenti, S. Midollini, A. Orlandini, A. Ienco, A. Vacca, J. Chem. Soc. Dalton Trans. (1996) 2821–2826.
[7] T.A. Albright, J.K. Burdett, M.-H. Whangbo, Orbital Interactions in Chemistry, second ed., John Wiley & Sons, Inc., New Jersey, 2013.
[8] F. Weinhold, C.R. Landis, Valency and Bonding: A Natural Bond Orbital Donor-Acceptor Perspective, Cambridge University Press, UK, 2005.
[9] C.J. Ballhausen, H.B. Gray, Molecular Orbital Theory, an Introduction Lecture

Note and Reprint Volume, W. A. Benjamin, Inc, New York, 1965.
[10] J.P. Foster, F. Weinhold, J. Am. Chem. Soc. 102 (1980) 7211–7218.
[11] M. Wolfsberg, L.J. Helmholz, J. Chem. Phys. 20 (1952) 837–843.
[12] R. Hoffmann, J. Chem. Phys. 39 (1963) 1397–1412.
[13] L. Libit, R. Hoffmann, J. Am. Chem. Soc. 96 (1974) 1370–1383.
[14] M. Reiher, A. Wolf, Relativistic Quantum Chemistry, the Fundamental Theory of Molecular Science, Wiley-VCH Verlag GmbH & Co. KGaA, Weinheim, 2009.
[15] P. Pyykkö, Chem. Rev. 88 (1988) 563–594.
[16] P. Jutzi, Angew. Chem. Int. Ed. 14 (1975) 232–245.
[17] Y. Apeloig, Theoretical aspects of organosilicon compounds, in: S. Patai, Z. Rappoport (Eds.), The Chemistry of Organic Silicon Compounds, John Wiley & Sons, Ltd, Chichester, 1989, pp. 57–225.
[18] P. Glatzel, U. Bergmann, Coord. Chem. Rev. 249 (2005) 65–95.
[19] K.M. Lancaster, K.D. Finkelstein, S. DeBeer, Inorg. Chem. 50 (2011) 6767–6774.
[20] S.N. MacMilan, R.C. Walroth, D.M. Perry, T.J. Morsing, K.M. Lancaster, Inorg. Chem. 54 (2015) 205–214.
[21] N. Lee, T. Petrenko, U. Bergmann, F. Neese, S. DeBeer, J. Am. Chem. Soc. 132 (2010) 9715–9727.
[22] F.A. Cotton, G. Wilkinson, C.A. Murillo, M. Bochmann, Advanced Inorganic Chemistry, sixth ed., John Wiley & Sons, Inc., New York, 1999, p. 388.
[23] W.M. Haynes, T.J. Bruno, D.R. Lide (Eds.), CRC Handbook of Chemistry and Physics, 95th Ed., Internet Version, 2015, pp. 9–27.
[24] H.A. Bent, Chem. Rev. 61 (1961) 275–311.
[25] A. Schier, H. Schmidbaur, P-Donor Ligands, in: Encyclopedia of Inorganic Chemistry, Wiley-VCH, Weinheim, 2006.
[26] R.S. Rowland, R. Taylor, J. Phys. Chem. 100 (1996) 7384–7391.
[27] T.L. Brown, K.J. Lee, Coord. Chem. Rev. 128 (1993) 89–116.
[28] K.A. Bunten, L. Chen, A.L. Fernandez, A.J. Poë, Coord. Chem. Rev. 223–234 (2002) 41–51.
[29] R. Stomberg, Acta Chem. Scand. 23 (1969) 2755–2763.
[30] T. Yamaguchi, O. Lindqvist, Acta Chem. Scand. A 35 (1981) 811–814.
[31] P. Nockemann, G. Meyer, Z. Anorg. Allg. Chem. 629 (2003) 123–128.
[32] G. Herzberg, Electronic Spectra and Electronic Structure of Polyatomic Molecules, Van Nostrand, New York, 1966.
[33] S.C. Goel, M.Y. Chiang, W.E. Buhro, J. Am. Chem. Soc. 112 (1990) 6724–6725.
[34] V.I. Minkin, L.E. Novorozhkin, M.S. Korobov, Uspekhi Khim. 63 (1994) 303–326. Russ. Chem. Rev. 63 (1994), 289–311 and references therein.
[35] Y. Zhao, D.G. Truhlar, Theor. Chem. Acc. 120 (2008) 215–241.
[36] H. Yamamoto, O. Matsuoka, Bull. Univ. Electro. Comm. 5 (1992) 23.
[37] T. Noro, M. Sekiya, T. Koga, Theor. Chem. Acc. 109 (2003) 85–90.
[38] H. Tatewaki, T. Koga, J. Chem. Phys. 104 (1996) 8493–8499.
[39] T. Noro, M. Sekiya, T. Koga, Theor. Chem. Acc. 98 (1997) 25–32.
[40] H. Tatewaki, T. Koga, H. Takashima, Theor. Chem. Acc. 96 (1997) 243–247.
[41] M. Sekiya, T. Noro, T. Koga, H. Matsuyama, J. Mol. Struct. (Theochem) 451 (1998), 61–60.
[42] T. Koga, H. Tatewaki, H. Matsuyama, Y. Satoh, Theor. Chem. Acc. 102 (1999) 105–111.
[43] T. Noro, M. Sekiya, T. Koga, H. Matruyama, Theor. Chem. Acc. 104 (2000) 146–152.
[44] T. Koga, S. Yamamoto, T. Shimazaki, H. Tatewaki, Theor. Chem. Acc. 108 (2002) 41–45.
[45] Y. Osanai, M. Sekiya, T. Noro, T. Koga, Mol. Phys. 101 (2003) 65–71.
[46] D.A. Pantazis, X.-Y. Chen, C.R. Landis, F. Nesse, J. Chem. Theor. Comput. 4 (2008) 908–919.
[47] T.H. Dunning, J. Chem. Phys. 90 (1989) 1007–1023.
[48] M. Douglas, N.M. Kroll, Ann. Phys. 82 (1972) 89–155.
[49] T. Nakajima, K. Hirao, Chem. Rev. 112 (2012) 385–402.
[50] F. Weigend, R. Ahlrichs, Phys. Chem. Chem. Phys. 7 (2005) 3297–3305.
[51] M.W. Schmidt, K.K. Baldridge, J.A. Boatz, S.T. Elbert, M.S. Gordon, J.H. Jensen, S. Koseki, N. Matsunaga, K.A. Nguyen, S. Su, T.L. Windus, M. Dupuis, J.A. Montgomery, J. Comput. Chem. 14 (1993) 1347–1363.
[52] M.S. Gordon, M.W. Schmidt, Advances in electronic structure theory: GAMESS a decade later, in: C.E. Dykstra, G. Frenking, K.S. Kim, G.E. Scuseria (Eds.), Theory and Applications of Computational Chemistry: the First Forty Years, Elsevier, Amsterdam, 2005.
[53] F. Neese, WIREs Comput. Mol. Sci. 2 (2012) 73–78.